Clinical Cancer Research

Low-Dose Histone Deacetylase Inhibitor Treatment Leads to Tumor Growth Arrest and Multi-Lineage Differentiation of Malignant Rhabdoid Tumors

Andrea Muscat[1,2], Dean Popovski[3,4], W. Samantha N. Jayasekara[3,4], Fernando J. Rossello[5,6], Melissa Ferguson[1,2], Kieren D. Marini[3,4], Muhammad Alamgeer[3,7], Elizabeth M. Algar[3,4], Peter Downie[8,9], D. Neil Watkins[3,4,10], Jason E. Cain[3,4], and David M. Ashley[1,2]

Abstract

Purpose: Malignant rhabdoid tumor (MRT) and atypical teratoid rhabdoid tumors (ATRT) are rare aggressive undifferentiated tumors primarily affecting the kidney and CNS of infants and young children. MRT are almost exclusively characterized by homozygous deletion or inactivation of the chromatin remodeling gene *SMARCB1*. SMARCB1 protein loss leads to direct impairment of chromatin remodeling and we have previously reported a role for this protein in histone acetylation. This provided the rationale for investigating the therapeutic potential of histone deactylase inhibitors (HDACi) in MRT.

Experimental Design: Whereas previously HDACis have been used at doses and schedules that induce cytotoxicity, in the current studies we have tested the hypothesis, both *in vitro* and *in vivo*, that sustained treatment of human MRT with low-dose HDACi can lead to sustained cell growth arrest and differentiation.

Results: Sustained low-dose panobinostat (LBH589) treatment led to changes in cellular morphology associated with a marked increase in the induction of neural, renal, and osteoblast differentiation pathways. Genome-wide transcriptional profiling highlighted differential gene expression supporting multilineage differentiation. Using mouse xenograft models, sustained low-dose LBH589 treatment caused tumor growth arrest associated with tumor calcification detectable by X-ray imaging. Histological analysis of LBH589-treated tumors revealed significant regions of ossification, confirmed by Alizarin Red staining. Immunohistochemical analysis showed increased TUJ1 and PAX2 staining suggestive of neuronal and renal differentiation, respectively.

Conclusions: Low-dose HDACi treatment can terminally differentiate MRT tumor cells and reduce their ability to self-renew. The use of low-dose HDACi as a novel therapeutic approach warrants further investigation. *Clin Cancer Res; 22(14); 3560–70.* ©*2016 AACR.*

[1]Cancer Services, Barwon Health, Geelong, Victoria, Australia. [2]School of Medicine, Deakin University, Geelong, Victoria, Australia. [3]Centre for Cancer Research, Hudson Institute of Medical Research, Clayton, Victoria, Australia. [4]Department of Molecular and Translational Science, Monash University, Clayton, Victoria, Australia. [5]Australian Regenerative Medicine Institute, Monash University, Clayton, Victoria, Australia. [6]Department of Anatomy and Developmental Biology, Monash University, Clayton, Victoria, Australia. [7]Department of Medical Oncology, Monash Medical Centre, East Bentleigh, Victoria, Australia. [8]Children's Cancer Centre, Monash Children's Hospital, Monash Health, Victoria, Australia. [9]Department of Paediatrics, Monash University, Clayton, Victoria, Australia. [10]The Kinghorn Cancer Centre, Garvan Institute of Medical Research, Darlinghurst, New South Wales, Australia.

Note: Supplementary data for this article are available at Clinical Cancer Research Online (http://clincancerres.aacrjournals.org/).

A. Muscat, D. Popovski, J.E. Cain, and D.M. Ashley contributed equally to this article.

Corresponding Authors: David M. Ashley, Cancer Services, Barwon Health, 70 Swanston Street, PO Box 281, Geelong, Victoria, Australia, 3220. Phone: 3-4215 2778; Fax: 3-4215-2836; E-mail: david.ashley@barwonhealth.org.au; and Jason E. Cain, Centre for Cancer Research, Hudson Institute of Medical Research, 27-31 Wright St, Clayton, Victoria 3168, Australia. Phone: 3-9902-4725; Fax: 3-9594-7114; E-mail: Jason.cain@hudson.org.au

doi: 10.1158/1078-0432.CCR-15-2260

Introduction

Malignant rhabdoid tumor (MRT) is a highly aggressive undifferentiated tumor occurring in infancy and early childhood and primarily affects the kidney and central nervous system (CNS; refs. 1–3). Current treatment for MRT includes surgical resection, chemotherapy, and radiotherapy with the average 5-year survival rate ranging from 8% to 12% (1, 4).

MRT is genetically defined by the inactivation of the SWI/SNF-related, matrix-associated, actin-dependent regulator of chromatin, subfamily b, member 1 (*SMARCB1*) gene. *SMARCB1* encodes a core subunit of the human ortholog of the Switch/Sucrose Non Fermentable (SWI/SNF) complex. MRT are classified by the complete or partial loss of the *SMARCB1* gene on both alleles via inactivating mutations, deletion or allelic loss of chromosome 22q (3). Aside from genomic alterations that lead to inactivation of *SMARCB1*, MRT is characterized by a remarkably stable genome having the lowest base rate change among all sequenced cancer types (5–7). This suggests that SMARCB1 inactivation alone is sufficient to initiate MRT, raising the possibility of epigenetic deregulation as causative in the development and pathogenesis of this disease.

We have previously shown that several HDACi can mimic the histone acetylation function of SWI/SNF complexes in SMARCB1-

Translational Relevance

Malignant rhabdoid tumor (MRT) is a rare aggressive undifferentiated tumor primarily affecting the kidney and CNS of infants and young children with a poor outcome using conventional approaches. Loss of the SMARCB1 protein, the hallmark of MRT, leads to direct impairment of chromatin remodeling, and we have previously reported a role for this protein in histone acetylation. This has provided the rationale for investigating the therapeutic potential of histone deactylase inhibitors (HDACi) in MRT. Whereas previously HDACis have been used at doses and schedules that induce cytotoxicity, we have now tested the hypothesis that sustained treatment of human MRT with low-dose HDACi can reprogram transcriptional profiles and lead to sustained cell growth arrest and differentiation. The innovative use of low-dose HDACi as differentiation therapy has major potential translational therapeutic implications in humans for both MRT and other epigenetically driven primitive solid tumors.

null cells and also provided evidence for direct epigenetic regulation of target gene promoters by SMARCB1 (8–10).

The immature phenotype of MRT, expression of many transcription factors and markers associated with stem cell networks, and the potential of MRT cells to differentiate to some degree along various lineages have been reported (11–13). In particular, SMARCB1 is required in the SWI/SNF chromatin remodeling complex for controlling the differentiation potential of MRT cells (14–16). Furthermore, mounting evidence supports a role for SMARCB1 and functional chromatin remodeling complexes in cellular lineage commitment and differentiation, including myogenic (15, 17), adipogenic (18), and erythropoietic (19) differentiation pathways.

Several studies now suggest that histone acetylation events are a key element of SMARCB1 function and MRT pathogenesis, leading to the study of histone de-acetylase inhibitors as potential therapy for MRT (8, 20–24). However, these studies have focused on HDACi as "cytotoxics" rather than differentiating agents.

The differentiating potential of HDACi was initially described in murine erythroleukemia cells in 1975 (25, 26). More recently, the ability of suberoylanilide hydroxamic acid (SAHA/vorinostat) and trichostatin A to induce mammary gland differentiation of human breast cancer cells suggests that solid tumors are also susceptible to HDACi-dependent differentiation (27, 28). Our recent data in osteosarcoma, a poorly differentiated tumor of bone, have suggested that lower doses of HDACi may prove effective and clinically viable (29).

Here, we examined the effects of low-dose LBH589 (panobinostat) treatment in long-term culture of human MRT cell lines and in mouse xenograft models. Our studies demonstrate that sustained exposure of MRT cell lines to low-dose LBH589 induces cell-cycle arrest and gene expression profiles consistent with renal, neuronal and osteoblast differentiation. In mouse xenograft models, continuous low-dose treatment with LBH589 resulted in a cytostatic tumor response accompanied by intratumoral bone deposition and induction of renal and neuronal gene expression. The capacity of MRT cells to undergo terminal differentiation in response to HDACi highlights the therapeutic potential of differentiating agents in the treatment of rhabdoid and other tumors.

Materials and Methods

Cell culture

STM91-01 and SJSC MRT cell lines were provided by Dr. Jaclyn Biegel (Children's Hospital of Philadelphia). Authenticated G401 was obtained from the American Type Culture Collection. All MRT lines were maintained in 5A McCoys 1x Modified Media (Sigma-Aldrich) supplemented with 10% fetal calf serum (FCS) and 1x glutamax in a humidified 5% CO_2/95% air atmosphere at 37°C. LBH589 (5 mmol/L; Novartis Pharmaceuticals) was prepared in 100% DMSO and stored in aliquots at −20°C. Appropriate dilutions were made into culture medium for experimental analyses. Culture media and reagents were replaced every 3 days. Genomic DNA from all cell lines was analyzed for deletions of *SMARCB1* by Multiplex Ligation-dependent Probe Amplification (MLPA), conducted by the Genetics and Molecular Pathology Laboratory, Monash Health (Melbourne, Australia). Absence of *SMARCB1* expression was further confirmed by RTPCR and Western blotting as previously described (8).

Cell viability

Cell viability was assessed using the colorimetric CellTitre 96Aqueous One Solution Cell Proliferation Assay (Promega) as instructed by the manufacturer. Cells were plated in 96-well plates at a density of 5×10^3 cells/well and allowed to adhere overnight. Cells were then treated for up to 72 hours with increasing concentrations of LBH589 or DMSO vehicle. Viability was determined at 0, 48, and 72 hours after treatment. MTS tetrazolium compound was added to the medium and incubated with cells at 37°C for 2 hours to allow cell-mediated reduction of MTS. Absorbance was measured at 490 nm. A reference wavelength of 620 nm was used for subtraction of background absorbance. Drug concentrations that achieved 50% growth inhibition (GI_{50}) were calculated as described previously (21).

Analysis of cell cycle and cell death

Cell-cycle analysis was performed as detailed previously (8). For analysis of cell death, 6×10^4 cells/well were plated in 24-well plates and allowed to adhere overnight. Cells were treated for 48 hours and then both adherent and supernatant cells were collected, washed in PBS and resuspended in PBS containing 50 μg/mL of propidium iodide (PI). Flow cytometry was performed using a LSRII analyzer (Becton Dickinson) and PI positivity was analyzed using the FACS Diva software program.

Protein acetylation

A total of 5×10^5 cells/well were plated in 6-well plates, allowed to adhere overnight and treated with 1, 5, 10, 20, 50, and 100 nmol/L LBH589 or DMSO vehicle for 24 hours. Cells were washed twice in ice-cold PBS and treated with RIPA lysis Buffer (1% NP-40, 0.1% SDS, 1% sodium deoxycholate, 150 mmol/L NaCl and buffered in 25 mmol/L Tris–HCl pH 7.6 with addition of protease and phosphatase inhibitor cocktails). Cells were collected in an eppendorf tube and incubated on ice for 10 minutes and then sonicated for 2 cycles of 30 seconds on, 30 seconds off at a setting of 5 on a XL-2000 series sonicator (Misonix). Cells were then centrifuged at 15,000 rpm for 15 minutes at 4°C and the supernatant collected. Protein quantification was performed using the DC Protein Assay (Bio-Rad) as per the manufacturer's instructions. Protein acetylation was determined by Western blot analysis on whole-cell lysates, separated on a 4% to 12% Tris-Bis gel

(Invitrogen) and transferred to a nitrocellulose membrane (Hybond-C Extra, GE Healthcare). Blots were probed with anti-rabbit Acetyl-Histone H3 (Cell Signaling Technology, no. 9675S), anti-rabbit Acetyl-Histone H4 (Cell Signaling Technology, no. 2591S), anti-rabbit Acetyl-α- Tubulin (Cell Signaling Technology, no. 5335P), and anti-mouse Actin (Abcam, ab2380) followed by donkey anti-mouse IRDye 680LT (Li-Cor Biosciences, no. 926-68022) and donkey anti-rabbit IRDye 800 CW (no. 926-32213) secondary antibodies and visualized via an Odessey Infrared Imaging System (v3.0, LI-COR). Densitometric analysis of Ac-H3 and Ac-H4 bands, normalized to Actin, was performed using Odyssey Infrared Imaging System software.

Senescence-associated β-Gal staining

Following 21 days of treatment, cultured cells were rinsed three times in PBS, and fixed in lacZ fix solution (0.2% glutaraldehyde, 2% buffered formalin), washed three times in PBS and then incubated in lacZ staining solution (1 mg/mL X-gal, 15 mmol/L potassium ferrocyanide and potassium ferricyanide, 6 mmol/L $MgCl_2$, 450 mmol/L NaCl buffered in citric acid/phosphate pH 6.0) at 37°C overnight protected from light.

Clonogenic assay

Complete methylcellulose media were prepared by adding McCoy's 5A modified media supplemented with 10% FCS and 1× glutamax to H4100 MethoCult methylcellulose base (Stem Cell Technologies), followed by vigorous shaking. The complete media were allowed to settle, and then aliquots were dispensed using a sterile luer lock syringe and 16-gauge blunt-end needle and stored at −20°C. Prepared aliquots were thawed just prior to use. Cells that had been treated for 21 days were harvested, and the cell density was adjusted to 1×10^4 cells/mL in fresh culture media. A 1:10 ratio of cell suspension to complete methylcellulose media was vigorously mixed and then allowed to settle to eliminate any air bubbles. A total volume of 2 mL was dispensed over 8 wells of a 24-well plate using a sterile syringe and 16-gauge blunt-end needle. Plates were incubated at 37°C in a humidified incubator with 5%CO_2 in air for 15 days. Colonies were stained with 0.005% crystal violet, and colonies containing >50 cells were counted under an inverted microscope. Biologic triplicate experiments were performed.

Global gene expression analysis

G401, SJSC, and STM91-01 cells were collected from 100-mm culture dishes following 21 days culture in the presence of LBH589 or vehicle. Biologic triplicate cultures were analyzed. RNA was extracted from cell pellets using the RNeasy Mini Kit (Qiagen) according to the manufacturer's instructions, including an on-column DNase digestion step. Microarray analysis of RNA was performed by the Australian Genome Research Facility (Melbourne, Australia). RNA quality and integrity was assessed using the Agilent Bioanalyzer 2100 and all samples scored a RIN≥7.0. 500 ng of total RNA per sample was processed and hybridized to Illumina Human HT-12v4 expression beadchips targeting in excess of 47,000 transcripts and known splice variants. Primary gene expression data are available on the Gene Expression Omnibus (GEO) public database (accession number GSE76664). Analysis of microarray data was performed as previously described (29). Venn diagrams were constructed using BioVenn (30). Gene Ontology Network analysis was performed using the ClueGO plugin of the open-source Cytoscape platform (31). ClueGo displays a functionally related network based on the categorization of differentially expressed genes into gene ontology groups. Gene ontology analysis of individual cell lines was performed using Partek Genomics Suite as previously described (29). Specific analysis of conserved gene ontology for biologic processes was performed using the ClueGo plugin of the Cytoscape platform.

Gene expression validation

RNA (500 ng) was reverse transcribed with random primers (pd(N)6; Amersham Pharmacia Biotech) and M-MLV reverse transcriptase RNaseH minus (Promega Corporation). Real-time Q-PCR reactions were performed using the 2xSensimix HRM kit (Quantace) with EvaGreen according to the manufacturer's instructions. Reactions were set up in triplicate using the QIAgility robotic system and were then run on a Rotor-gene Q real-time thermal cycler (QIAGEN). Primer details are listed in Supplementary Table S1. Cycling was 95°C for 10 minutes followed by at least 40 cycles of 95°C for 10 seconds, 60°C for 15 seconds and 72°C for 15 seconds. For *β2MG* and *GUSB* the annealing temperature was adjusted to 57°C. A melt step (62°C–95°C rising by 1°C/cycle) upon completion of cycling was included to confirm the presence of a single amplicon. Comparative quantitation analysis was undertaken using the Rotor-Gene Q series software. An additional control was included in every run for use as a calibrator. Data for each gene was normalized to the average expression of three housekeeping genes (*β2MG*, *HPRT*, and *GUSB*), which were examined by real-time Q-PCR under the same conditions.

Qualitative analysis of osteoblast differentiation

A total of 5×10^5 cells/well were plated in 6-well plates and allowed to adhere overnight. Cells were then treated with LBH589 (10 nmol/L G401 and SJSC, 20 nmol/L STM91-01) or DMSO vehicle for 21 days. Culture media and reagents were replaced daily and cells were passaged when they reached 80% confluency. For qualitative analysis of osteoblast differentiation, cultures were washed in PBS, fixed in 10% buffered formalin at RT for 15 minutes, rinsed three times with dH_2O and stained with Alizarin Red (2%, pH 4.1, Sigma-Aldrich) for 10 minutes at RT on a platform rocker. Excess stain was removed by repeated washes with dH_2O.

Human MRT xenograft model

A total of 1×10^6 MRT cells (G401 or SJSC) where injected into the flanks of female BALB/c, 6–8 weeks of age, athymic nude mice (Animal Resources Centre, Australia). Cells were resuspended in 100 μL of 1:1 mixed cell suspension and Matrigel. Tumor size was measured daily using digital calipers, and volumes were calculated according to the formula: Tumor volume (mm^3) = ($Width^2$ × Length)/2. Once tumors reached a volume of 150–200 mm^3, mice were randomized to receive low-dose LBH589 (5 mg/kg) or vehicle control (5% dextrose). Mice were treated daily by intraperitoneal injection for 21 or 28 days or until ethical endpoints were reached. Ethical endpoints include tumor volume of 800 mm^3, >10% body weight loss or signs of general ill-health. At the completion of the study, mice were euthanized in a carbondioxide chamber and tissue was harvested from the flanks for histology and analysis of differentiation markers by immunohistochemistry. A small cohort of vehicle and LBH589-treated mice ($n = 3$) were immediately imaged using the Feinfocus Y. Cougar Microfocus X-ray Inspection System (YXLON). Tumors from these mice were removed for whole tumor Alizarin Red staining. Briefly,

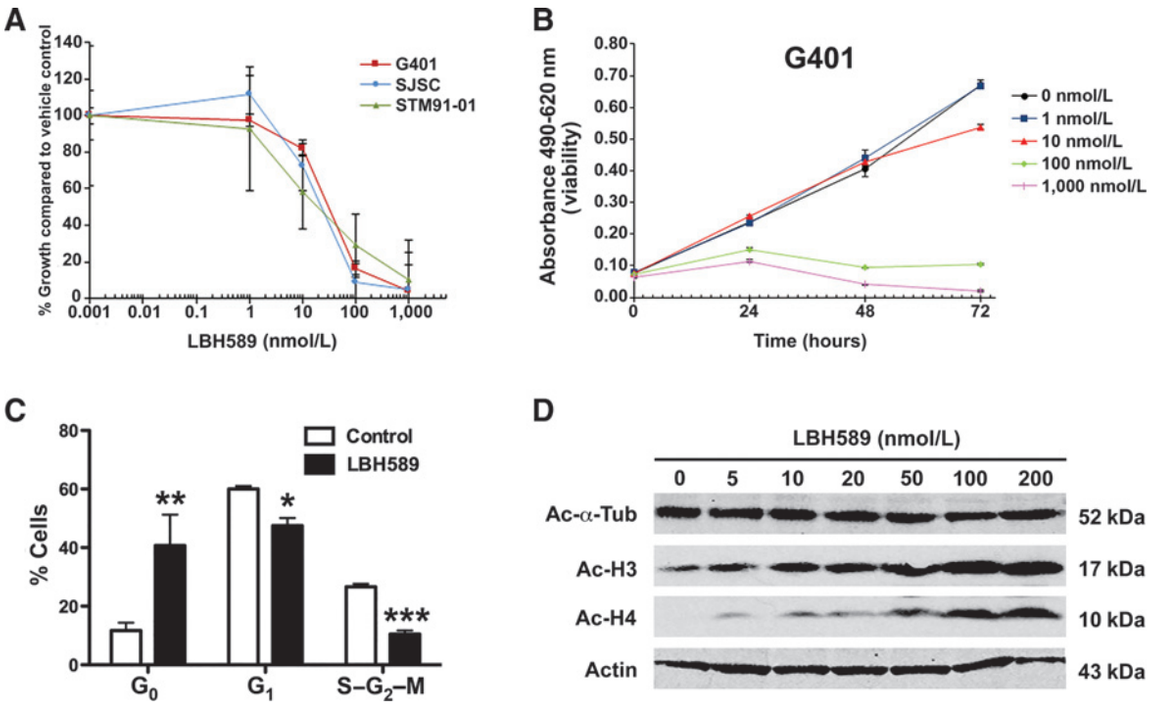

Figure 1.
LBH589 inhibits MRT cell growth and upregulates the acetylation of histones. A, growth curve of human MRT cell lines treated with increasing concentrations of LBH589 for 72 hours. Data represent mean ± SEM of biologic triplicate experiments. B, cell viability of G401 cells treated with increasing concentrations of LBH589 and analyzed over a 72-hour period. Data represent mean ± SEM of biologic triplicates. C, cell-cycle analysis of G401 cells treated with LBH589. Data represent mean ± SEM of biologic triplicate experiments. *, $P < 0.05$; **, $P < 0.01$; ***, $P < 0.001$. D, Western blot analysis of acetylated proteins in G401 cells treated with increasing concentrations of LBH589 for 24 hours.

tumors were fixed in 100% ethanol for 24 hours, transferred into 100% acetone for 24 hours, and stained in Alizarin Red (0.1%) for 4 days at 37°C. Following rinsing in dH20, tumors were incubated in 1% KOH until tumor soft tissue had digested. Tumors were then transferred through a series of glycerol/KOH washes (20%/1%, 50%/1%, 80%/1%) before being stored in 80% glycerol.

All experiments involving animals were approved in advance by an Animal Ethics Committee at Monash University and were carried out in accordance with "Australian Code of Practice for the Care and Use of Animals for Scientific Purposes."

Histology and immunohistochemistry

Formalin-fixed, paraffin-embedded tumor sections were analyzed by histology after generating 4-μm tissue sections and staining with hematoxylin and eosin or Alizarin Red. Immunohistochemical stains were performed on representative formalin-fixed paraffin-embedded tumor sections using Acetyl-Histone H3 (Cell Signaling Technology, no. 9675S), Acetyl-Histone H4 (Cell Signaling Technology, no. 2591S), PAX2 (Covance, PRB-276P) and cleaved caspase-3 (Cell Signaling Technology, no. 9661), TUJ1 (Covance, MMS-435P), and PCNA (DAKO, M0879) antibodies. Following sodium citrate (pH 6.0) antigen retrieval, staining was performed as detailed in the Vectastain ABC Elite Rabbit IgG Kit or M.O.MTM Kit (Vector Laboratories). The detection system used the standard strepdavidin–biotin peroxidase complex with 3, 3 diaminobenzidine (Sigma). The slides were counterstained with hematoxylin and imaged using a Nikon DS-Fil H550S bright-field photomicroscope.

Statistical analysis

GraphPad Prism 5.0c (GraphPad Software) was used to statistically analyses the data. Data were analyzed by a two-tailed Student *t* test or one-way ANOVA, and a probability score equal to or less than 0.05 was considered to indicate statistical significance.

Results

Human MRT cell lines are highly sensitive to LBH589-induced growth arrest

To investigate the therapeutic potential of HDACi in MRT, we first cultured a panel of established human MRT cell lines (G401, SJSC, and STM91-01) in increasing concentrations of the potent pan-deacetylase inhibitor LBH589. Assessment of cell viability using MTS assays demonstrated that continuous exposure of G401, SJSC, and STM91-01 cell lines to LBH589 resulted in a dose-dependent reduction in cell viability with a GI_{50} of 56 ± 5 nmol/L, 69 ± 5 nmol/L and 66 ± 15 nmol/L, respectively, following 72 hours treatment (Fig. 1A and B; Supplementary Fig. S1A and B). Concentrations of LBH589 as low as 10 nmol/L caused 18 ± 4% ($P = 0.00569$), 27 ± 3% ($P = 0.00031$) and 36 ± 7% ($P = 0.00268$) growth inhibition compared to vehicle control of G401, SJSC and STM91-01 cells, respectively, within 72 hours (Fig. 1A and B; Supplementary Fig. S1A and B). Cell-cycle analysis revealed that 10 nmol/L LBH589 treatment for 72 hours was sufficient to arrest G401 cells, resulting in an increased proportion of cells

in G_0 (vehicle, 12% ± 3% vs. LBH589, 41% ± 11%, $P = 0.00142$) and a reduction in the proportion of cells in G_1 (vehicle, 60% ± 1% vs. LBH589, 48% ± 3%, $P = 0.01144$) and S–G_2–M (vehicle, 27% ± 1% vs. LBH589, 11% ± 1%, $P = 0.00049$; Fig. 1C). Similar results were also observed for SJSC (23% increase in G_0 cells) and STM91-01 (12% increase in G_0 cells; Supplementary Fig. S1C and D). However, higher concentrations of LBH589 were necessary to elicit a death response in these cells. Indeed, analysis of cell death following 48-hour treatment, measured by PI exclusion, revealed negligible death of cells treated with 10 nmol/L LBH589 (Supplementary Fig. S1E). These data also showed that STM91-01 cells were the most resistant of the cell lines, requiring a higher concentration of drug to trigger cell death. Additionally, assessment of the pan-HDACi SAHA revealed a similar effect on the growth profile of the MRT cell lines, although 1,000-fold higher concentrations were required to induce a response (Supplementary Fig. S1F–H).

To assess the on-target effects of LBH589, acetylation of the non-histone protein α-tubulin, and acetylation of histone H3 and histone H4 protein was determined by Western blot analysis following 24 hours treatment with increasing LBH589 concentrations (5–200 nmol/L). In contrast to studies in other cells (29, 32), acetylation of α-tubulin was already detected strongly in untreated MRT cells and no further increase was apparent upon treatment in any of the cell lines (Fig. 1D; Supplementary Fig. S2A and B). This is also consistent with previous studies that identify class I HDACs as significantly differentially expressed in ATRT (33) rather than class II HDACs such as HDAC6 that have been found to modulate acetylation of α-tubulin (34). The increase in acetylated histone H3 and acetylated histone H4 expression corresponded with increasing concentrations of LBH589 (Fig. 1D and Supplementary Fig. S2A–S2E). An increase in both acetylated histone H3 and acetylated histone H4 was detected after treatment with as little as 5 nmol/L LBH589. A more noticeable induction of acetylated histones was evident in cells treated with 10 to 20 nmol/L LBH589, correlating with the concentration at which cell-cycle arrest was observed. Maximal acetylation of histone H3 and histone H4 was achieved by treatment with 50 to 100 nmol/L LBH589.

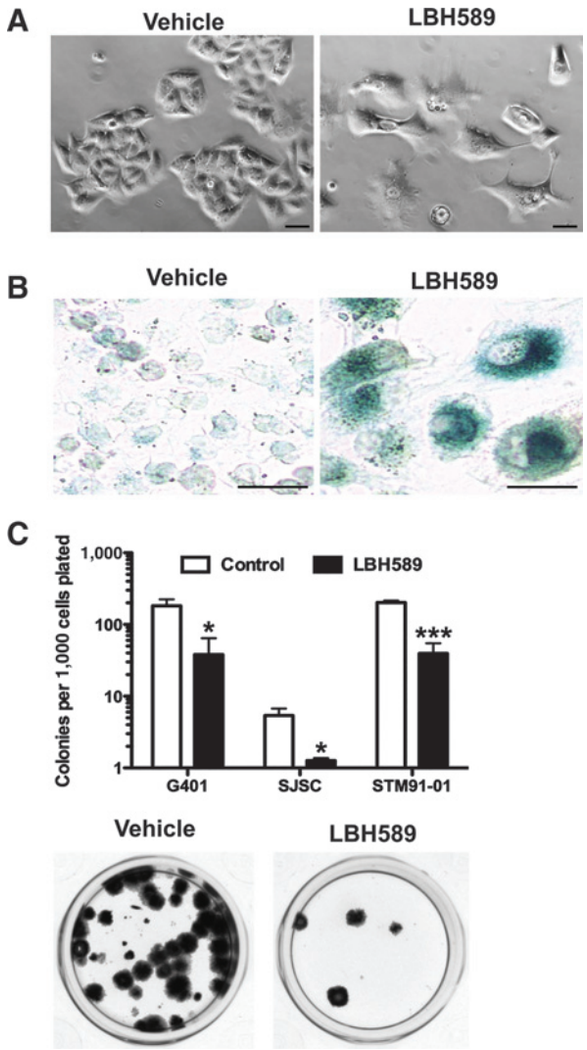

Figure 2.
Sustained low-dose LBH589 promotes cellular senescence and inhibits self-renewal in MRT cells. A, phase-contrast microscopy of G401 cells following 21 days of sustained treatment with 10 nmol/L LBH589. Scale bar, 100 μm. B, senescence-associated β-galactosidase staining of G401 cells. Scale bar, 100 μm. C, clonogenic assay of G401 and SJSC cells pretreated with 10 nmol/L LBH589 for 21 days and STM91-01 cells pretreated with 20 nmol/L LBH589 for 28 days. Mean ± SEM. *, $P < 0.05$; ***, $P < 0.001$ (top). Crystal violet stained G401 cell colonies (bottom).

Sustained low-dose LBH589 treatment promotes cellular senescence and inhibits the self-renewal capacity of MRT cells

LBH589 treatment concentrations of 10 nmol/L (G401 and SJSC) and 20 nmol/L (STM91-01) were selected on the basis that they induced arrest of cell growth without triggering a cell death response and increased the acetylation of histone proteins. The arrest of cells in G_0 phase of the cell-cycle is indicative of cellular senescence. Indeed, sustained culture of G401, SJSC, and STM91-01 cells in the presence of a sub-lethal dose of LBH589 inhibited cell proliferation and induced cellular senescence. A corresponding change in cellular morphology was observed, characterized by a flattened and enlarged phenotype and the occasional presence of cellular projections (Fig. 2A). Additionally, the number of cells positive for senescence-associated β-galactosidase was increased (Fig. 2B; Supplementary Fig. S3A). Importantly, all of the cell lines cultured in the presence of LBH589 remained viable throughout the culture period. To assess whether low-dose LBH589 affects clonal growth of MRT, G401 and SJSC cell lines were cultured in the presence of 10 nmol/L LBH589 or vehicle control for 21 days and plated at low density in methycellulose. Colony formation was significantly inhibited in both G401 and SJSC cells (4.8-fold and 4.2-fold decrease, respectively, $P < 0.05$) following LBH589 treatment (Fig. 2C; Supplementary Fig. S3B). Similarly, STM91-01 cells cultured in 20 nmol/L LBH589 for 28 days exhibited a similar reduction in colony number (5.1-fold decrease, $P < 0.01$; Fig. 2C; Supplementary Fig. S3B). The inhibitory effect on colony formation was replicated in G401 cells using 1 μmol/L SAHA over 21 days (Supplementary Fig. S3C). Together, these findings suggest that low-dose LBH589 potently inhibits MRT self-renewal, impedes cell proliferation, and promotes cell-cycle arrest.

Low-dose LBH589 induces global gene expression changes consistent with cell growth arrest and differentiation

Growth arrest, altered cellular morphology, and reduced self-renewal of MRT cells following sustained treatment *in vitro* with low-dose LBH589 is consistent with traits of cellular differentiation. Because the MRT cell of origin remains undefined and G401 (renal tumor), SJSC (liver tumor), and STM91-01 (lung metastasis of a renal tumor) cell lines were derived from tumors that arose in different tissue sites, we investigated potential LBH589-mediated lineage differentiation. To determine changes in global gene expression following 21 days culture in the presence of low-dose LBH589, we performed genome-wide transcriptional profiling of G401, SJSC, and STM91-01 using the HumanHT-12 v4 Expression BeadChip (Illumina), which contains 47,231 probes representing over 31,000 annotated genes. Principal component analysis (PCA) of microarray data revealed modest variability within biological replicates but a marked separation between the DMSO vehicle control and LBH589 treatment groups for each cell line (Fig. 3A; Supplementary Fig. S4). Hierarchical cluster analysis identified 473 (67 downregulated and 406 upregulated), 383 (129 downregulated and 254 upregulated), and 501 (84 downregulated and 417 upregulated) differentially expressed genes in G401, SJSC, and STM91-01 low-dose LBH589-treated cells, respectively (Fig. 3B; Supplementary Fig. S4; Supplementary Tables S2–S4). Of these, 30 genes were conserved between all cell lines and 159 were conserved in at least two cell lines (Fig. 3C). Remarkably, gene ontology analysis of differentially expressed genes revealed that 67% (482/719) were conserved between G401, SJSC, and STM91-01 and 82% were conserved in at least two cell lines (Fig. 3D; Supplementary Fig. S5; Supplementary Tables S5 and S6). These data strongly suggest that uniquely differentially expressed genes in each cell line converge on common gene ontology functional groups. Detailed analysis of gene ontology tables and network maps revealed enrichment of functional groups predominantly associated with cell proliferation and cell-cycle regulation (Fig. 3E; Supplementary Fig. S5; Supplementary Tables S6–S9) and multilineage differentiation (Fig. 3F; Supplementary Fig. S5; Supplementary Tables S6–S9).

Detailed inspection of G401 cell-cycle-related functional groups revealed enrichment for genes that are required during cell-cycle progression. These were downregulated following LBH589 treatment and included genes essential for DNA replication and synthesis (*PRIM2A*, *RRM2*; Fig. 3E). In contrast, genes upregulated following LBH589 treatment included negative regulators of cell-cycle and promoters of cell-cycle arrest (*PLK2*, *SFN*, *CDKN1A*, *CDKN2A*, *GADD45A*, *BTG4*, *SASH1*, and *PDGFRL*; Fig. 3E).

The observed changes in cellular morphology and G_0 growth arrest were also potential signs of terminal cell differentiation. As mentioned, gene ontology analysis showed enrichment of functional groups associated with multilineage differentiation, including but not limited to hematopoiesis, angiogenesis, myogenesis, osteogenesis, neurogenesis, and renal morphogenesis (Supplementary Fig. S5; Supplementary Tables S6–S9). Functional groups associated with renal and hepatic differentiation were more frequently observed in G401 and SJSC, respectively, consistent with their site of origin. However, renal and neuronal development and differentiation, in particular, were enriched in all cell lines irrespective of their tissue of origin (G401 data are presented in Fig. 3F). Because MRT predominantly affects the kidneys and brains of infants, we interrogated the functional groups associated with renal morphogesis and neurogenesis in more detail.

FGF20, required for the maintenance of embryonic nephron progenitors, is markedly downregulated following LBH589 treatment in G401 cells. Similarly, genes associated with the progression of renal morphogenesis (*FZD4*, *FOXD1*, and *COL4A5*) were upregulated consistent with induction of renal differentiation. Likewise, genes required for neuronal migration, differentiation, and function were upregulated, while inhibitors of neurotransmission and synaptogenesis were downregulated following LBH589 treatment, indicative of neuronal development (Fig. 3F).

We observed conserved functional groups associated with osteogenesis, including but not limited to bone remodeling, bone mineralization, regulation of ossification, and osteoblast differentiation, in all three cell lines. Because we have previously shown the potential of low-dose LBH589 to drive osteoblast differentiation in human osteosarcoma, we explored this in more detail in G401 cells. Notably, markers of mature bone (*SPP1*), genes associated with the promotion of bone differentiation and development (*PRRX2*, *SOX4*, *HAPLN1*, *PAPSS2*), and inhibitors of osteoclastogenesis (*TCTA*) were upregulated following LBH589 treatment (Fig. 4A). In order to investigate upregulation of osteogenesis-related genes, quantitative real-time PCR for a panel of known osteoblast differentiation markers and regulators revealed increased expression of osteblast precursors (*RUNX2*, *SP7/Osterix)*, preosteoblasts (*COL1A1*, *BMP7*, *ALPL*), and mature osteoblasts (*IBSP/Bone sialoprotein, TNFRSF11B/Osteoprotegerin*) with varying degrees of significance across all of the human MRT cell lines assayed and was also observed for G401 cells treated with SAHA (Fig. 4B; Supplementary Fig. S6A–C). Furthermore, culture of G401 cells in the presence of 10 nmol/L LBH589 for 21 days resulted in positive staining by Alizarin Red, a marker of mineralized extracellular matrix. (Fig. 4C). Collectively, these data show that, in addition to predicted renal, hepatic, and neuronal differentiation, low-dose LBH589 drives osteoblast differentiation of human MRT cells.

Low-Dose LBH589 Arrests Tumor Growth and Drives Multilineage Differentiation *In Vivo*

The therapeutic potential of sustained low-dose LBH589 on MRT *in vivo* was investigated using xenograft models for G401 and SJSC. Following the injection of 1×10^6 cells into the flanks of athymic nude mice, a 95% (19/20) and 47% (7/15) tumor engraftment rate was observed in G401 and SJSC injected mice, respectively. Tumors reached a volume of $\sim$200 mm^3 2 to 4 weeks following inoculation, and mice were randomized to receive vehicle control or 5 mg/kg of LBH589 daily by intraperitoneal injections. This dose is well below the maximum tolerated dose of 15 mg/kg (Novartis, personal communication) and we have previously demonstrated this dose to be efficacious in an osteosarcoma model without leading to systemic toxicity (28). G401 and SJSC tumors in mice treated with vehicle control grew rapidly and reached endpoint tumor volume of 800 mm^3 within 12 to 20 days following the commencement of treatment (Fig. 5A and B; Supplementary Fig. S6D). In contrast, tumors in mice treated with 5 mg/kg LBH589 underwent a complete growth arrest, and in the case of SJSC even showed a reduction in tumor size (Fig. 5A and B; Supplementary Fig. S6E). LBH589-treated tumors remained well-defined, spherical in appearance and hardened over the treatment duration. Importantly, body weight was unaffected in LBH589-

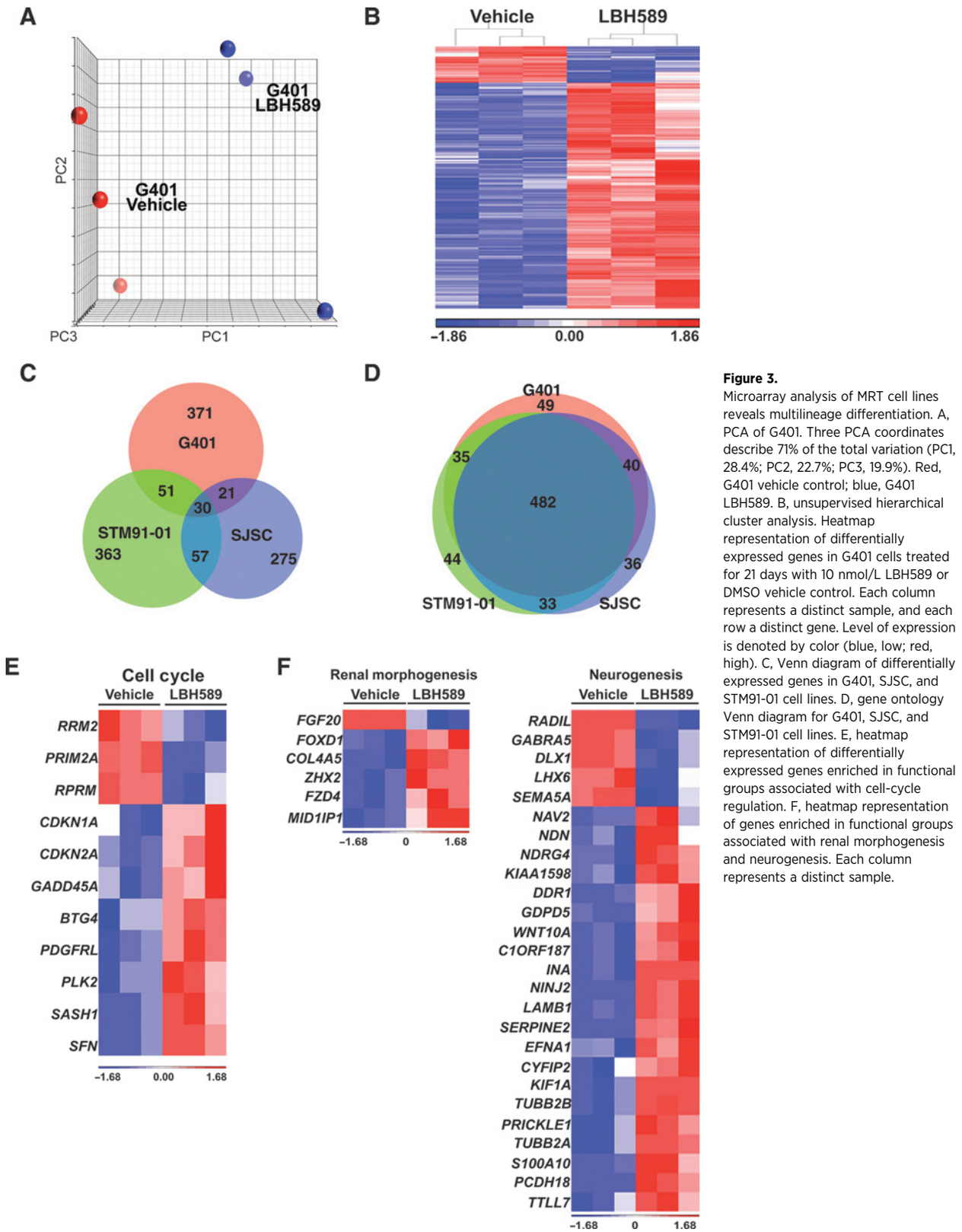

Figure 3.
Microarray analysis of MRT cell lines reveals multilineage differentiation. A, PCA of G401. Three PCA coordinates describe 71% of the total variation (PC1, 28.4%; PC2, 22.7%; PC3, 19.9%). Red, G401 vehicle control; blue, G401 LBH589. B, unsupervised hierarchical cluster analysis. Heatmap representation of differentially expressed genes in G401 cells treated for 21 days with 10 nmol/L LBH589 or DMSO vehicle control. Each column represents a distinct sample, and each row a distinct gene. Level of expression is denoted by color (blue, low; red, high). C, Venn diagram of differentially expressed genes in G401, SJSC, and STM91-01 cell lines. D, gene ontology Venn diagram for G401, SJSC, and STM91-01 cell lines. E, heatmap representation of differentially expressed genes enriched in functional groups associated with cell-cycle regulation. F, heatmap representation of genes enriched in functional groups associated with renal morphogenesis and neurogenesis. Each column represents a distinct sample.

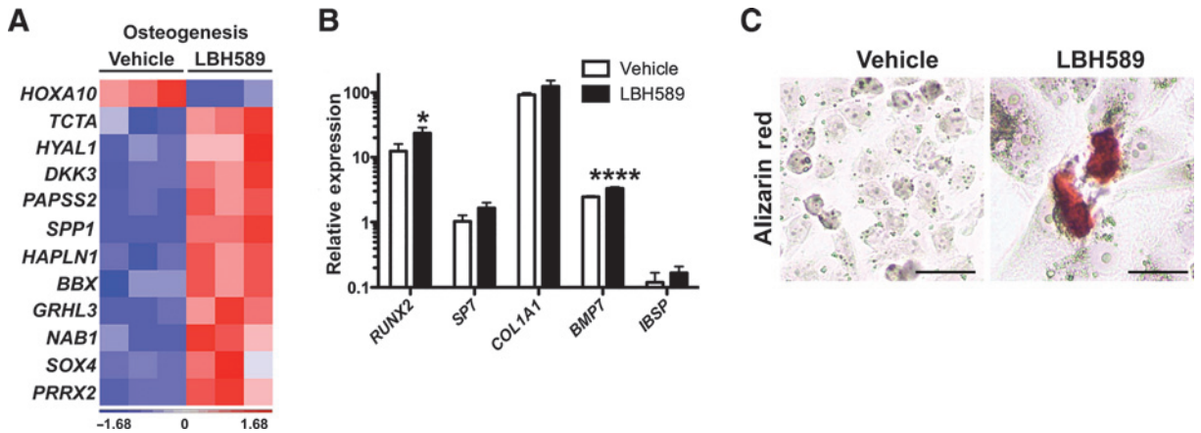

Figure 4.

LBH589 treatment results in gene expression changes associated with osteoblast differentiation and bone formation. A, heatmap representation of genes enriched in functional groups associated with osteogenesis. B, quantitative real-time PCR of G401 cells cultured for 21 days in the presence of 10 nmol/L LBH589 for the expression of osteoblast differentiation markers. *, $P < 0.05$; ****, $P < 0.0001$. C, Alizarin red staining of G401 cells following 21 days of treatment with 10 nmol/L LBH589. Scale bar, 100 μm.

treated mice, suggesting that the treatment was well tolerated and did not cause systemic toxicity (Fig. 5C and D). Following 28 days of continuous treatment, immunohistochemical analysis of G401 and SJSC tumor tissue showed a 2.1-fold ($P < 0.001$) and 2.7-fold ($P < 0.01$) reduction in cell proliferation, respectively, as determined by PCNA staining (Fig. 5E). In addition, LBH589 treatment led to a significant increase of acetylated histone H3 (G401, $P < 0.001$; SJSC, $P < 0.05$) and acetylated histone H4 (G401, $P < 0.0001$; SJSC, $P = 0.0001$) consistent with *in vitro* findings and demonstrating biological activity of LBH589 in these *in vivo* models (Fig. 5F and G).

Histologic analysis of G401 and SJSC xenograft tumors revealed typical rhabdoid tumor morphology with large eccentrically located nuclei and abundant eosinophillic cytoplasm (35). X-ray imaging of a small cohort of LBH589-treated mice with G401 or SJSC xenografts showed evidence of intratumoral ossification that was absent in vehicle controls (Fig. 6A). Remarkably, analysis of H&E-stained sections from LBH589-treated tumors exhibited areas of dense bone deposition (Fig. 6B). Bone differentiation in LBH589-treated tumors was confirmed by staining with Alizarin Red (Fig. 6C). Bone deposition was rarely observed in vehicle control tumors by H&E or Alizarin Red staining. To evaluate this further, we performed whole-tumor staining with Alizarin Red. Consistent with analysis of tumor sections and X-ray imaging, an intricate network of mineralized bone was observed in LBH589-treated tumors following digestion of the soft tissue (Supplementary Fig. S6F and G). Furthermore, quantitative PCR revealed a marked increase in the expression of osteoblast differentiation markers in LBH589-treated tumors, including a significant 3.8-fold increase in the preosteoblast marker *COL1A1* ($P < 0.05$) and a 3.3-fold increase in the mature osteoblast marker bone sialoprotein (*IBSP*, $P < 0.01$; Supplementary Fig. S6H).

In addition to bone differentiation, *in vitro* gene expression analysis also suggested LBH589-induced renal and neuronal differentiation. In order to assess renal differentiation in G401 and SJSC tumors, we examined the expression of PAX2, a marker of renal mesenchymal–epithelial transition, by immunohistochemistry. PAX2 expression was markedly increased in G401 and SJSC tumors following sustained LBH589 treatment (Fig. 6D). The expression of TUJ1, a marker of mature neurons, was observed in both G401 and SJSC vehicle- and LBH589-treated tumors. However, while TUJ1 was relatively evenly distributed throughout the vehicle controls, TUJ1 staining was predominantly confined to dense, localized areas within the LBH589-treated tumors, consistent with focal differentiation (Fig. 6E). Positive staining for cleaved caspase-3, used as an indicative measure of apoptosis, was unchanged in SJSC, and only a modest (2-fold, $P < 0.05$) increase was observed in G401 (Supplementary Fig. S7). These findings suggest that low-dose LBH589 inhibits MRT tumor growth *in vivo* by inhibiting cell proliferation and driving multilineage differentiation, specifically along the bone, renal, and neuronal lineages.

Discussion

MRT/ATRT is a rare cancer; however, it is responsible for substantial morbidity and mortality. Outcomes are poor, particularly after recurrence, highlighting the urgent need for new and improved therapies. HDACi are an emerging class of anticancer agents with activity in hematologic malignancies (36). To date, evidence of impact on solid malignancies is lacking, and significant adverse effects associated with doses required to elicit a desired cytotoxic effect have limited their applications, particularly in children where MRT/ATRT predominately occurs.

Here, we have identified that sublethal, low doses of the HDACi LBH589 act as a potent inducer of MRT cell differentiation. Culture of human MRT cell lines with low-dose LBH589 inhibits cell growth and clonogenicity, induces cell-cycle arrest and senescence, and results in terminal differentiation into mature, bone-forming osteoblasts. LBH589 treatment of a mouse xenograft model of MRT resulted in a significant inhibition of tumor growth and increased the expression of differentiation markers in the absence of any detectable sign of toxicity in the animals.

Evidence of disrupted differentiation in MRT

MRTs are a heterogeneous tumor characterized by variable amounts of primitive neuronal ectoderm, mesenchymal, and epithelial elements. This phenotype is suggestive of the hypothesis that MRTs may arise from pluripotent embryonic stem cell

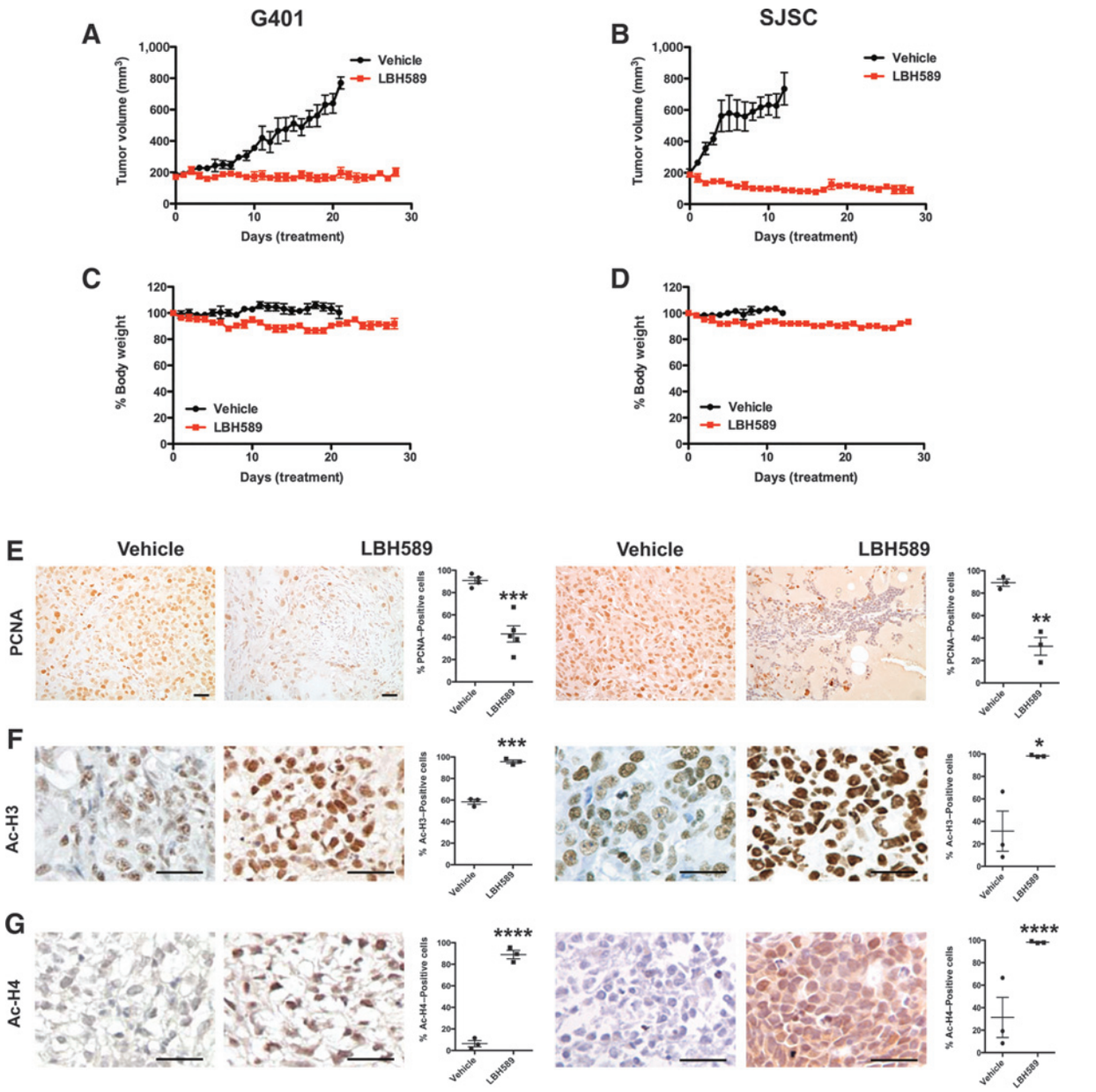

Figure 5.
LBH589 inhibits MRT cell growth *in vivo*. Xenograft flank tumors of G401 and SJSC treated with 5 mg/kg LBH589 i.p. daily for 28 days. A, B, tumor volume. Mean ± SEM. C, D, percentage of body weight. Mean ± SEM. Immunohistochemical analysis of G401 and SJSC xenograft tissue for PCNA (E), acetylated-Histone H3 (F), and acetylated-Histone H4 (G). *, $P < 0.05$; **, $P < 0.01$; ***, $P < 0.001$; ****, $P < 0.0001$. Scale bar, 200 μm.

precursors (13). In support of this hypothesis, Venneti and colleagues demonstrated that a number of stem cell transcription factors, such as Oct4, UTF1, TCL1, and Zpf206, are present in both MRT and ATRT, with Zpf206 significantly upregulated in ATRT. Importantly, the critical finding was not just the elevated levels of stem cell transcription factors; it was the lack of traditional germ cell factors, such as PLAP, AFP, and B-HCG, in MRT that they believed was indicative of an incomplete lineage differentiation.

The loss of the SWI/SNF chromatin remodeling complex and SMARCB1 itself may be essential for the lack of differentiation potential of MRT cells (14–16). In fact, mounting evidence supports a role for SMARCB1 and functional chromatin remodeling complexes in cellular lineage commitment and differentiation, including myogenic (15, 17), adipogenic (18), and erythropoietic (19) differentiation pathways.

HDAC inhibitor activity in MRT

We and others have previously shown that HDACi can mimic the histone acetylation function of SWI/SNF complexes in SMARCB1-null cells (8, 9) and promote transcriptional activity

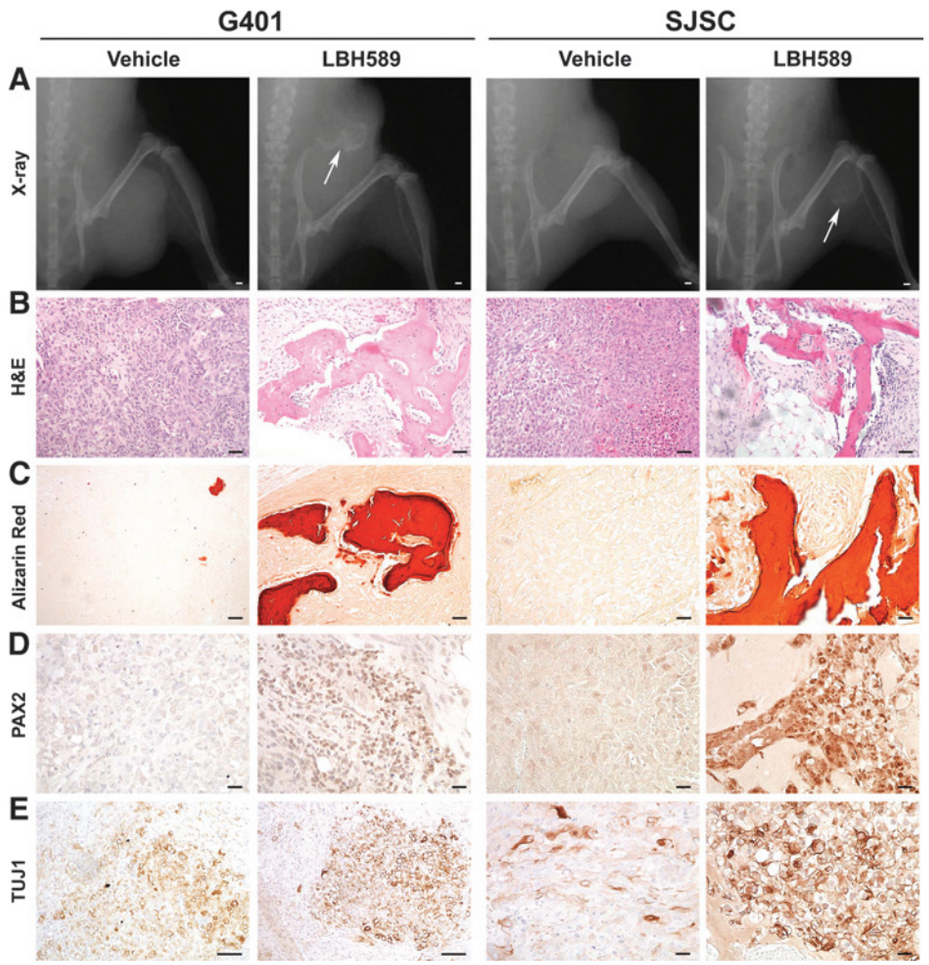

Figure 6.
LBH589 drives multilineage differentiation of MRT xenografts. Xenograft flank tumors of G401 and SJSC treated with 5 mg/kg LBH589 i.p. daily for 28 days. X-ray imaging (A, scale bar, 1000 μm; arrow, region of calcification), hematoxylin and eosin (B), Alizarin Red (C), PAX2 (D), and TUJ1 (E) immunohistochemistry in G401 and SJSC xenograft flank tumors treated with 5 mg/kg of LBH589 i.p. daily for 28 days. Scale bar, 200 μm.

from target promoters that are otherwise silenced in MRT. These positive data were supported by other studies using *in vivo* models, with most mice responding favorably to treatment protocols incorporating HDACi (29, 37).

Conclusion

While the precise mechanism by which this HDACi is able to promote differentiation at low dose remains to be determined, this may provide an effective and well-tolerated therapeutic option for the treatment of MRT and likely other solid tumors with similarly undifferentiated phenotypes.

As a next step, future studies could now be considered that utilize HDACi as maintenance differentiating therapy following the more conventional administration of radiation or cytotoxic chemotherapies.

Disclosure of Potential Conflicts of Interest

No potential conflicts of interest were disclosed.

Authors' Contributions

Conception and design: A. Muscat, D.N. Watkins, J.E. Cain, D.M. Ashley
Development of methodology: A. Muscat, W.S.N. Jayasekara, M. Ferguson, D.N. Watkins, J.E. Cain, D.M. Ashley
Acquisition of data (provided animals, acquired and managed patients, provided facilities, etc.): A. Muscat, D. Popovski, W.S.N. Jayasekara, M. Ferguson, M. Alamgeer, E.M. Algar, P. Downie, J.E. Cain, D.M. Ashley
Analysis and interpretation of data (e.g., statistical analysis, biostatistics, computational analysis): A. Muscat, D. Popovski, F.J. Rossello, M. Ferguson, K.D. Marini, M. Alamgeer, E.M. Algar, J.E. Cain, D.M. Ashley
Writing, review, and/or revision of the manuscript: A. Muscat, D. Popovski, F.J. Rossello, M. Ferguson, K.D. Marini, M. Alamgeer, E.M. Algar, P. Downie, D.N. Watkins, J.E. Cain, D.M. Ashley
Administrative, technical, or material support (i.e., reporting or organizing data, constructing databases): A. Muscat, D. Popovski, W.S.N. Jayasekara, M. Ferguson, M. Alamgeer, E.M. Algar, J.E. Cain, D.M. Ashley
Study supervision: E.M. Algar, D.N. Watkins, J.E. Cain, D.M. Ashley

Acknowledgments

The authors thank Novartis for supplying LBH589.

Grant Support

The work was supported by the Bailey's Day Charity (J.E. Cain and D. Popovski), the Victorian Cancer Agency (D.M. Ashley, A. Muscat, and M. Ferguson) and the Victorian Government's Operational Infrastructure Support Program. The costs of publication of this article were defrayed in part by the payment of page charges. This article must therefore be hereby marked *advertisement* in accordance with 18 U.S.C. Section 1734 solely to indicate this fact.

The costs of publication of this article were defrayed in part by the payment of page charges. This article must therefore be hereby marked advertisement in accordance with 18 U.S.C. Section 1734 solely to indicate this fact.

Received September 30, 2015; revised January 27, 2016; accepted February 10, 2016; published OnlineFirst February 26, 2016.

References

1. Bikowska B, Grajkowska W, Jozwiak J. Atypical teratoid/rhabdoid tumor: short clinical description and insight into possible mechanism of the disease. Eur J Neurol 2011;18:813–8.
2. Serowka K, Chiu Y. Central nervous system (CNS) tumors in the first six months of life: the Childrens Hospital Los Angeles Experience, 1979–2005. Pediatr Hematol Oncol 2010;27:90–102.
3. Versteege I, Sévenet N, Lange J, Rousseau-Merck MF, Ambros P, Handgretinger R, et al. Truncating mutations of hSNF5/INI1 in aggressive paediatric cancer. Nature 1998;394:203–206.
4. Athale UH, Duckworth J, Odame I, Barr R. Childhood atypical teratoid rhabdoid tumor of the central nervous system: a meta-analysis of observational studies. Pediatr Hematol Oncol 2009;9:651–63.
5. Hasselblatt M, Isken S, Linge A, Eikmeier K, Jeibmann A, Oyen F, et al. High-resolution genomic analysis suggests the absence of recurrent genomic alterations other than SMARCB1 aberrations in atypical teratoid/rhabdoid tumors. Genes Chromosomes Cancer 2013;52:185–90.
6. Lee RS, Stewart C, Carter SL, Ambrogio L, Cibulskis K, Sougnez C, et al. A remarkably simple genome underlies highly malignant pediatric rhabdoid cancers. J Clin Invest 2012;122:2983–8.
7. McKenna ES, Sansam CG, Cho YJ, Greulich H, Evans JA, Thom CS, et al. Loss of the epigenetic tumor suppressor SNF5 leads to cancer without genomic instability. Mol Cell Biol 2008;28:6223–33.
8. Algar EM, Muscat A, Dagar V, Rickert C, Chow CW, Biegel JA, et al. Imprinted CDKN1C is a tumor suppressor in rhabdoid tumor and activated by restoration of SMARCB1 and histone deacetylase inhibitors. PLoS One 2009;4:e4482.
9. Yamamichi N, Yamamichi-Nishina M, Mizutani T, Watanabe H, Minoguchi S, Kobayashi N, et al. The Brm gene suppressed at the post-transcriptional level in various human cell lines is inducible by transient HDAC inhibitor treatment, which exhibits antioncogenic potential. Oncogene 2005;24:5471–81.
10. West AC, Johnstone RW. New and emerging HDAC inhibitors for cancer treatment. J Clin Invest 2014;124:30–39.
11. Deisch J, Raisanen J, Rakheja D. Immunohistochemical expression of embryonic stem cell markers in malignant rhabdoid tumors. Pediatr Dev Pathol 2011;14:353–9.
12. Okuno K, Ohta S, Kato H, Taga T, Sugita K, Takeuchi Y. Expression of neural stem cell markers in malignant rhabdoid tumor cell lines. Oncol Rep 2010;23:485–92.
13. Venneti S, Le P, Martinez D, Xie SX, Sullivan LM, Rorke-Adams LB, et al. Malignant rhabdoid tumors express stem cell factors, which relate to the expression of EZH2 and Id proteins. Am J Surg Pathol 2011;35:1463–72.
14. Albanese P, Belin MF, Delattre O. The tumour suppressor hSNF5/INI1 controls the differentiation potential of malignant rhabdoid cells. Eur J Cancer 2006;42:2326–34.
15. Joliot V, Ait-Mohamed O, Battisti V, Pontis J, Philipot O, Robin P, et al. The SWI/SNF subunit/tumor suppressor BAF47/INI1 is essential in cell cycle arrest upon skeletal muscle terminal differentiation. PLoS One 2014;9:e108858.
16. Wei D, Goldfarb D, Song S, Cannon C, Yan F, Sakellariou-Thompson D, et al. SNF5/INI1 deficiency redefines chromatin remodeling complex composition during tumor development. Mol Cancer Res 2014;12:1574–85.
17. Roy K, de la Serna IL, Imbalzano AN. The myogenic basic helix–loop–helix family of transcription factors shows similar requirements for SWI/SNF chromatin remodeling enzymes during muscle differentiation in culture. J Biol Chem 2002;277:33818–24.
18. Caramel J, Medjkane S, Quignon F, Delattre O. The requirement for SNF5/INI1 in adipocyte differentiation highlights new features of malignant rhabdoid tumors. Oncogene 2008;27:2035–44.
19. Griffin CT, Brennan J, Magnuson T. The chromatin-remodeling enzyme BRG1 plays an essential role in primitive erythropoiesis and vascular development. Development 2008;135:493–500.
20. Blattmann C, Oertel S, Thiemann M, Weber KJ, Schmezer P, Zelezny O, et al. Suberoylanilide hydroxamic acid affects gammaH2AX expression in osteosarcoma, atypical teratoid rhabdoid tumor and normal tissue cell lines after irradiation. Strahlenther Onkol 2012;188:168–76.
21. Furchert SE, Lanvers-Kaminsky C, Juurgens H, Jung M, Loidl A, Fruhwald MC. Inhibitors of histone deacetylases as potential therapeutic tools for high-risk embryonal tumors of the nervous system of childhood. Int J Cancer 2007;120:1787–94.
22. Graham C, Tucker C, Creech J, Favours E, Billups CA, Liu T, et al. Evaluation of the antitumor efficacy, pharmacokinetics, and pharmacodynamics of the histone deacetylase inhibitor depsipeptide in childhood cancer models *in vivo*. Clin Cancer Res 2006;12:223–34.
23. Jaboin J, Wild J, Hamidi H, Khanna C, Kim CJ, Robey R, et al. MS-27-275, an inhibitor of histone deacetylase, has marked in vitro and *in vivo* antitumor activity against pediatric solid tumors. Cancer Res 2002;62:6108–15.
24. Wagner JM, Hackanson B, Lubbert M, Jung M. Histone deacetylase (HDAC) inhibitors in recent clinical trials for cancer therapy. Clin Epigenetics 2010;1:117–36.
25. Leder A, Leder P. Butyric acid, a potent inducer of erythroid differentiation in cultured erythroleukemic cells. Cell 1975;5:319–22.
26. Leder A, Orkin S, Leder P. Differentiation of erythroleukemic cells in the presence of inhibitors of DNA synthesis. Science 1975;190:893–4.
27. Munster PN, Troso-Sandoval T, Rosen N, Rifkind R, Marks PA, Richon VM. The histone deacetylase inhibitor suberoylanilide hydroxamic acid induces differentiation of human breast cancer cells. Cancer Res 2001;61:8492–7.
28. Vigushin DM, Ali S, Pace PE, Mirsaidi N, Ito K, Adcock I, et al. Trichostatin A is a histone deacetylase inhibitor with potent antitumor activity against breast cancer *in vivo*. Clin Cancer Res 2001;7:971–6.
29. Cain JE, McCaw A, Jayasekara WS, Rossello FJ, Marini KD, Irving AT, et al. Sustained low-dose treatment with the histone deacetylase inhibitor LBH589 induces terminal differentiation of osteosarcoma cells. Sarcoma 2013;2013:608964.
30. Hulsen T, de Vlieg J, Alkema W. BioVenn - a web application for the comparison and visualization of biological lists using area-proportional Venn diagrams. BMC Genomics 2008;9:488.
31. Bindea G, Mlecnik B, Hackl H, Charoentong P, Tosolini M, Kirilovsky A, et al. ClueGO: a cytoscape plug-in to decipher functionally grouped gene ontology and pathway annotation networks. Bioinformatics 2009;25:1091–3.
32. Iancu-Rubin C, Gajzer D, Mosoyan G, Feller F, Mascarenhas J, Hoffman R. Panobinostat (LBH589)-induced acetylation of tubulin impairs megakaryocyte maturation and platelet formation. Exp Hematol 2012;40:564–74.
33. Sredni ST, Halpern AL, Hamm CA, Bonaldo Mde F, Tomita T. Histone deacetylases expression in atypical teratoid rhabdoid tumors. Childs Nerv Syst 2013;29:5–9.
34. Zhang Y, Li N, Caron C, Matthias G, Hess D, Khochbin S, et al. HDAC-6 interacts with and deacetylates tubulin and microtubules *in vivo*. EMBO J 2003;22:1168–79.
35. Parwani AV, Stelow EB, Pambuccian SE, Burger PC, Ali SZ. Atypical teratoid/rhabdoid tumor of the brain: cytopathologic characteristics and differential diagnosis. Cancer 2005;105:65–70.
36. Azad N, Zahnow CA, Rudin CM, Baylin SB. The future of epigenetic therapy in solid tumours—lessons from the past. Nat Rev Clin Oncol 2013;10:256–66.
37. Rai M, Soragni E, Jenssen K, Burnett R, Herman D, Coppola G, et al. HDAC inhibitors correct Frataxin deficiency in a Friedreich ataxia mouse model. PLoS One 2008;3:e1958.